Earth Surface Mineral dust source InvesTigation (EMIT)

EMIT L3 Algorithm: Aggregated Mineral Spectral Abundance

Theoretical Basis

Gregory S. Okin, Francisco Ochoa
Department of Geography, University of California, Los Angeles
Philip G. Brodrick, David R. Thompson
Jet Propulsion Laboratory, California Institute of Technology
Abigail Keebler, Bethany L. Ehlmann
California Institute of Technology
Natalie Mahowald
Cornell University
Ron Miller
Goddard Institute for Space Studies

Version 1.0

Aug 2023

Jet Propulsion Laboratory
California Institute of Technology
Pasadena, California 91109-8099

Change Log

Version	Date	Comments
0.1	Oct, 2019	Initial Draft
0.2	Jan 2020	Post-PDR refinements
0.3	Feb 2020	Refinements from demo SDS
0.4	Feb 2022	Refinements from January 2022 Science Team Meeting
1.0	Aug 2023	First release.

TABLE OF CONTENTS

1. Key Teammembers

A large number of individuals contributed to the development of the algorithms, methods, and implementation of the L3 approach for EMIT. The primary contributors are the following:

- Philip G. Brodrick (Jet Propulsion Laboratory)
- Gregory S. Okin (UCLA)
- Francisco Ochoa (UCLA)
- David R. Thompson (Jet Propulsion Laboratory)
- Roger Clark (Planetary Science Institute)
- Kathleen Grant (USC)
- Robert O. Green (Jet Propulsion Laboratory)
- Bethany L. Ehlmann (California Institute of Technology)
- Abigail Keebler (California Institute of Technology)
- Ron Miller (GISS)
- Natalie Mahowald (Cornell University)
- Paul Ginoux (GFDL)
- Carlos Pérez García-Pando (BSC)
- Maria Goncalves (BSC)
- Robert O. Green (Jet Propulsion Laboratory)

2. Historical Context and Background on the EMIT Mission and its Instrumentation

Mineral dust aerosols originate as soil particles lifted into the atmosphere by wind erosion. Mineral dust created by human activity makes a large contribution to the uncertainty of direct radiative forcing (RF) by anthropogenic aerosols (USGCRP and IPCC). Mineral dust is a prominent aerosol constituent around the globe. However, we have poor understanding of its direct radiative effect, partly due to uncertainties in the dust mineral composition. Dust radiative forcing is highly dependent on its mineral-specific absorption properties. The current range of iron oxide abundance in dust source models translates into a large range of values, even changing the sign of the forcing (-0.15 to 0.21 W/m2) predicted by Earth System Models (ESMs) (Li et al., 2020). The National Aeronautics and Space Administration (NASA) recently selected the Earth Surface Mineral Dust Source Investigation (EMIT) to close this knowledge gap. EMIT will launch an instrument to the International Space Station (ISS) to directly measure and map the soil mineral composition of critical dust-forming regions worldwide.

The EMIT Mission will use imaging spectroscopy across the visible shortwave (VSWIR) range to reveal distinctive mineral signatures, enabling rigorous mineral detection, quantification, and mapping. The overall investigation aims to achieve two objectives.

1. Constrain the sign and magnitude of dust-related RF at regional and global scales. EMIT achieves this objective by acquiring, validating and delivering updates of surface mineralogy used to initialize ESMs.
2. Predict the increase or decrease of available dust sources under future climate scenarios. EMIT achieves this objective by initializing ESM forecast models with the mineralogy of soils exposed within at-risk lands bordering arid dust source regions.

The EMIT instrument is a Dyson imaging spectrometer that will resolve the distinct absorption bands of iron oxides, clays, sulfates, carbonates, and other dust-forming minerals with contiguous spectroscopic measurements in the visible to short wavelength infrared region of the spectrum. EMIT will map mineralogy with a spatial sampling to detect minerals at the one-hectare scale and coarser, ensuring accurate characterization the mineralogy at the grid scale required by ESMs. EMIT's fine spatial sampling will resolves the soil exposed within hectare-scale agricultural plots and open lands of bordering arid regions, critical to understanding feedbacks caused by mineral dust arising from future changes in land use, land cover, precipitation, and regional climate forcing.

The EMIT Project is part of the Earth Venture-Instrument (EV-I) Program directed by the Program Director of the NASA Earth Science Division (ESD). EMIT is comprised of a Visible/Shortwave Infrared Dyson imaging spectrometer adapted for installation on the International Space Station (ISS).

Table 1 below describes the different data products to which the EMIT Mission will provide to data archives. This document describes the "Level 3" stage which relies on outputs from the Level 2A algorithms (cloud masking, standing water, vegetation cover) and the Level 2B mineral detection algorithms to produce aggregated mineral maps that can be ingested into Earth System models to evaluate Radiative Forcing (RF) impacts (Level 4).

Table 1. Emit Data Product Hierarchy

Data Product	**Description**	**Initial Availability**	**Median Latency Post-delivery**	**NASA DAAC**
Level 0	Raw collected telemetry	4 months after IOC	2 months	LP DAAC
Level 1a	Reconstructed, depacketized, uncompressed data, time referenced, annotated with ancillary information reassembled into scenes.	4 months after IOC	2 months	LP DAAC
Level 1b	Level 1a data processed to sensor units including geolocation and observation geometry information	4 months after IOC	2 months	LP DAAC
Level 2a	Surface reflectance derived by screening clouds and correction for atmospheric effects.	8 months after IOC	2 months	LP DAAC
Level 2b	Mineralogy derived from fitting reflectance spectra, screening for non-mineralogical components.	8 months after IOC	2 months	LP DAAC
Level 3	Gridded map of mineral composition aggregated from level 2b with uncertainties and quality flags	11 months after IOC	2 months	LP DAAC
Level 4	Earth System Model runs to address science objectives	16 months after IOC	2 months	LP DAAC

A high-level, yet complete workflow of the EMIT science data system is shown in Figure 1 for context.

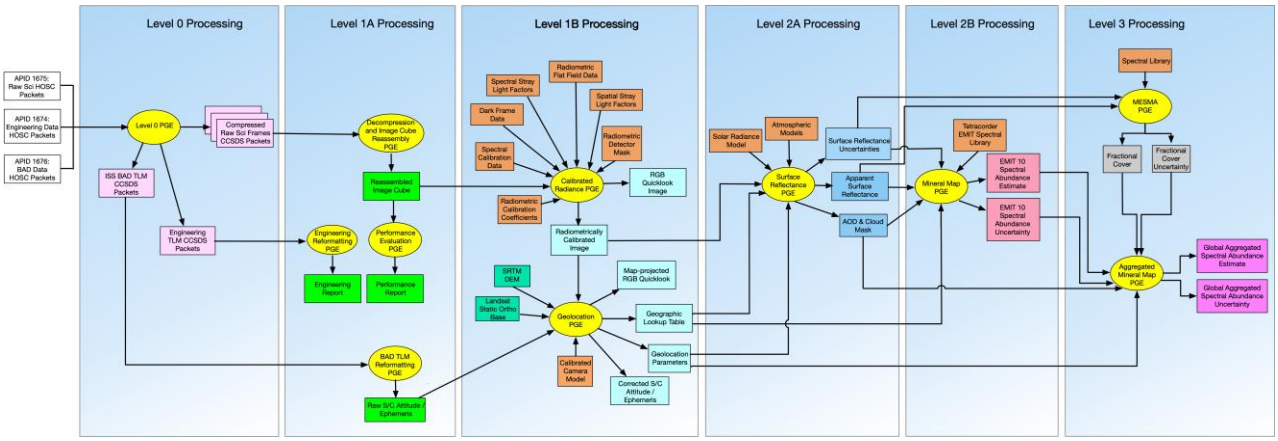

Figure 1. High-level workflow of the EMIT science data system.

3. Algorithm rationale

The EMIT L3 approach relies on the strength of the mineral detection algorithms described in L2B, which have a long development and verification history (e.g., Clark 2003, Swayze 1997). In the L3 step, these L2B products are adjusted for the sub-pixel vegetation and then aggregated to the half degree resolution required for L4 modeling. The aggregation step uses simple masked averaging, and as measurement noise propagated as inputs into L3 is expected to be random, uncertainties in this step should only decrease.

The main new algorithmic approach used in the L3 step is the sub-pixel vegetation fraction estimations, which are generated here using spectral unmixing. Like the mineral identification algorithms used, spectral unmixing has a long history of development and validation (e.g., Roberts et al., 1993). Also like the mineral identification, the strength of the detection lies in the endmember libraries used by the algorithm, as well as the mechanism for selecting endmembers during a retrieval. Multiple approaches to this challenge exist in the literature. These range from comparing the results of many combinations of low numbers of spectra, as in the Multiple Endmember Spectral Mixture Analysis (MESMA; Roberts 1998), to bootstrap selection of endmembers over a large random deck (autoMCU; Asner and Lobell, 2000). Endmember selection techniques have undergone a series of advancements (Dennison & Roberts, 2003; Dennison et al., 2004; Schaaf et al., 2011; Roth et al., 2012), and the resulting products from these advance spectral unmixing analyses have been field-validated and shown to be effective relative to other methods (Dennison et al., 2019). Here, we draw off of this work, using a simple unmixing approach with a limited endmember subset that utilizes a bootstrap over both endmembers and reflectance spectra (drawn over the reported range of reflectance uncertainty from L2A) in order to simultaneously estimate fractional cover and the corresponding uncertainty.

With unmixing complete, the L3 algorithm accounts for the bare soil fraction within a scene and aggregates spatially by tracking pixel location, handing acquisition overlaps, and using simple spatial averages.

4. Algorithm description

Below we detail the algorithms used to generate EMIT L3 products. The major processing steps, as well as input and output data, are outlined in Figure 1.

4.1 Input data

The EMIT input and output data products delivered to the DAAC use their formatting conventions, the system operates internally on data products stored as binary data cubes with detached human-readable ASCII header files. The precise formatting convention adheres to the ENVI standard, accessible (Jan 2020) at https://www.harrisgeospatial.com/docs/ENVIHeaderFiles.html. The header files all consist of data fields in equals-sign-separated pairs, and describe the layout of the file. In the file descriptions below, *n* denotes the number of lines particular to the given acquisition and *c* the number of columns.

The specific input files needed for the L3 stage are:

1. **Estimated mineral spectral abundance,** provided as *n* x *c* x 10 BIL interleave data cubes, where each band corresponds to the one of the 10 identified EMIT mineral classes. Each channel contains the estimated EMIT-10 mineral spectral abundance, as defined in L2B Section 4.2.2.
2. **Estimated mineral spectral abundance uncertainty,** provided as *n* x *c* x 10 BIL interleave data cubes, where each band corresponds to the one of the 10 identified EMIT mineral classes. Each channel contains the estimated EMIT-10 mineral spectral abundance uncertainty, as defined in L2B Section 5.
3. **Surface reflectance,** provided as *n* x *c* x *b* BIL interleave data cubes, where each of *b* bands corresponds to a different wavelength.
4. **Channelized surface reflectance uncertainty,** provided as *n* x *c* x *b* BIL interleave data cubes, where each of *b* bands corresponds to a different wavelength.
5. **Data quality mask,** provided as *n* x *c* x 7 binary files. Details on mask assignments are available in the L2A ATBD.
6. **Geospatial reference data,** provided as raw-space n x *c* x 3 BIL interleave data cubes. The three channels designate the x, y, z ground-coordinates of each pixel.

Note – for practical (disk storage) reasons, mosaics are first constructed of L2BMIN products (group 1 and group 2 mineral identification, band depth, and uncertainty), rather than the mineral spectral abundance. After mosaics are constructed, the conversion occurs – however there is no functional difference between the two, so we describe the process as if the mosaicing occurred on mineral spectral abundance for clarity.

4.2 Theoretical description

To introduce the Level 3 aggregation, we first define the Spectral Abundance (SA) for an observed reflectance spectrum containing an absorption signature. The SA aims to estimate the effective areal fraction of the spectrum spatial footprint covered by the pure material. To estimate SA_i for mineral *i*, we calculate the distance from the deepest point of the mineral absorption to the local continuum and normalize it relative to the feature depth for a pure library spectrum of the material, and then scale by the proportion of mineral *i* in the library spectrum. It is a simple proxy for the areal coverage fraction of that mineral within the spectrum spatial footprint, relative to the library sample. Intimate mixtures count as aggregate materials which apportion their area to their constituent minerals. Note that at this time, as neither the particle size of the absorbing target material nor the surrounding parent material are considered, magnitude shifts may occur – in particular, it is quite likely the fine grained particles with strong absorption coefficients, such as iron oxides, are represented as larger than they really are. A future update to this document and the data product will aim to correct this. For a complete description of this process, we refer the reader to the EMIT L2B Mineral Detection and Related Products at the Pixel Scale Algorithm Theoretical Basis Document (ATBD). These values are provided as inputs into the Level 3 aggregation. The L3 aggregation step uses the 60 m ground-level resolution SA output from L2B,

in conjunction with various masks and adjustments for vegetation, in order to estimate the Aggregated Spectral Abundance (ASA) of each EMIT mineral for each ESM grid square. This L3 ASA product is defined as the expected normalized band depth that one would find upon measuring the surface reflectance at a random bare (not vegetated or within water) location within the grid square. Here we use "expectation" formally in its statistical sense to mean a numerical average.

Aggregation from the native-sensor resolution SA estimates to 0.5° x 0.5° model grid cells requires four basic steps: 1) the correction of mineral SA estimations to account for partial vegetation cover, 2) the conversion of raw-space input data products to map-space co-registered products, using provided geospatial information, 3) the aggregation of vegetation-corrected mineral SA to 0.5° x 0.5° model grid cell estimates, and 4) the propagation of uncertainty.

4.2.1 Bare Earth Percentage Adjustment

The goal of the L3 aggregation is to provide the Aggregated Spectral Abundance of the given mineral over only bare-ground regions of the half degree model grid cells. Consequently, prior to aggregation all areas that are not bare-ground need to be removed. This is done by first masking out areas where the soil fraction f_s, does not exceed a particular threshold $f_{s,th}$, caused by vegetation, shade, water, or anthropogenic sources obscuring the bare-ground. We select a $f_{s,th}$ value of 0.5 based on published evaluations (Okin *et al.*, 2001) and inspection of EMIT global mosaics. Masks from L2A (cloud, cirrus, water (all three phases), spacecraft, dilated clouds, and aerosol optical depth > 0.5 - see the L2A ATBD for more detail) are also applied at this step, as well as an additional mask for anthropogenic land used from Zanaga et al. (2022), as our endmember libraries are optimized for natural desert areas. In areas where $1 > f_s > f_{s,th}$, the SA of 60 m ground-level resolution L2B outputs must also be adjusted so that they are only representative of the soil fraction of the surface. This adjustment is proportional to the inverse of bare ground coverage, giving

$$SA_i^c = \frac{SA_i}{f_s} \quad (1)$$

where SA_i^c is the corrected spectral abundance.

To estimate fractional cover, we use a Monte Carlo Spectral Unmixing strategy, based on decades of literature (e.g., Roberts et al. 1998, Asner and Lobell 2000, and Dennison et al., 2019). Several key parameters, including the endmember selection strategy, observation normalization techniques, and the number of bootstrap samples were investigated. Simulation experiments comparing over one million synthetic spectra constructed with endmember holdout sets were utilized to select parameter values (generally following the approach of Okin et al., 2015). Selected parameter values are shown in Table 4.2.1-1. Parameters were chosen based on a combination of mean squared error, prediction variance, prediction bias, and computation time. All values can be tested through parameter selection in the unmix.jl script provided in the SpectralUnmixing EMIT SDS repository (https://github.com/emit-sds/SpectralUnmixing). A sample comparison between two scenarios is shown in Figure 4.3.1.-1.

Table 4.2.1-1 Unmixing Parameter Value Selection

Parameter Name	**Tested Values**	**Selected Value**
Endmember Selection	MESMA, Monte Carlo SMA	Monte Carlo SMA
Endmember Selection Order	Random, Class-Even	Class-Even

Normalization[1]	None, Brightness, 1070, 1500, 1756, 2030	Brightness
Maximum Number of Combinations (MESMA only)	10, 100, 500, 1000	NA
Number of Endmembers per Class per Bootstrap Draw (SMA only)	5, 10, 30, 50	10
Number of Bootstrap Draws	1, 5, 10, 20, 50, 100, 200	50

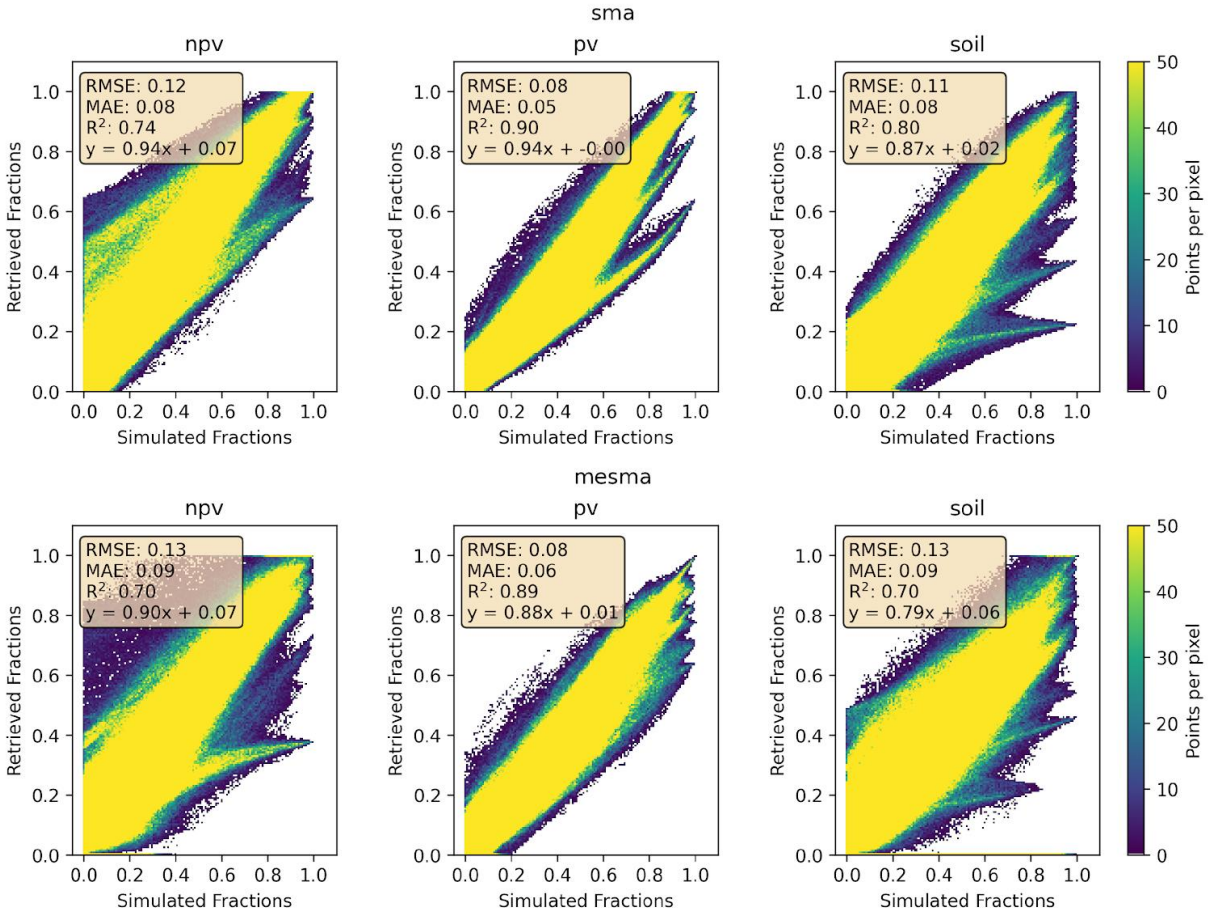

Figure 4.2.1-1. Comparison between two parameter combinations. On top is a Monte Carlo unmixing analysis with 10 endmembers per class per bootstrap draw, brightness normalization, class-even endmember selection, and 50 bootstrap draws. On the bottom is a MESMA-style unmixing analysis with a maximum of 1000 class-even selected endmembers, brightness normalization, and 50 bootstrap draws.

Three natural, dominant classes were utilized in the fractional cover unmixing: soil (including all bare exposed surface, such as mineral outcrops), photosynthetic vegetation, and nonphotosynthetic vegetation. Data from many arid regions around the globe were utilized to construct this endmember library, and scripts outlining the aggregation and downselection of endmembers are

[1] Normalization uses a constant factor to scale each spectrum. Brightness uses the two-norm, and the wavelengths scale to a constant at that wavelength.

available here: https://github.com/emit-sds/SpectralUnmixing. As noted above, other dominant classes (snow/ice, water, and urban cover) will all be identified through a separate procedure.

4.2.2 Orthorectification and mosaicing

To aggregate into 0.5° x 0.5° model grid cells, all data (NBD_i^c and associated masks) must be transformed from raw to map space. Since pixel-specific georeferencing has already occurred, here we use the reference pixel coordinates as a look up table to convert all products to map space. This is done on a line-by-line basis and many acquisitions will overlap. Consequently, acquisitions will be mosaiced after masking (including input cloud, shade, and water masks as well as derived vegetation masks (Section 4.2.1)), by selecting for pixels with the minimum solar zenith angle.

4.2.3 Aggregation

Half-degree spatial aggregates of the corrected spectral abundances are not intended to account for the variable vegetation, quartz, and feldspar distributions within a grid cell, given that these will enter into L4 models from other sources (e.g., Scanza et al., 2015). This aggregated product, which we term the Aggregated Spectral Abundance (ASA) and is calculated for each of the EMIT 10 minerals (*i*), is calculated as the simple average of relevant pixels within the grid, giving:

$$ASA_i = \frac{\sum_{j=1}^{N}(1-m_j)SA_{i,j}^c}{\sum_{j=1}^{N}(1-m_j)} \quad (2)$$

where *j* is an index over the two spatial dimensions within the given grid cell and m_j is a binary indication of whether each individual pixel is masked (either from any of the cloud, cloud cirrus, water, spacecraft interference, cloud dilation, or high aerosol input masks or because $f_s < f_{s,th}$).

The corresponding variability in ASA_i is characterized as

$$\sigma_i = \sqrt{\frac{\sum_{j=1}^{N}(1-m_j)\left(SA_{i,j}^c - ASA_i\right)^2}{-1+\sum_{j=1}^{N}(1-m_j)}} \quad (3)$$

where σ_i is the standard deviation of the estimates of ASA_i^c in each grid cell.

4.3 Practical Considerations

The various adjustment and aggregation code described above is implemented in Python 3.7, and can operate independently on different scenes. All computation is faster than the L1B, L2A, and L2B stages of analysis, limited mainly by the input / output throughput. Operations can be executed out-of-core to remove any memory limitations for long lines. Dependencies are all provided as input, making this code base easily operable and stand-alone.

4.4 Output Data

Level 3 output data include both *delivered* products, which are necessary for mission success, as well as *auxiliary* products, which are generated in the process of producing the delivered products, and preserved for transparency and issue tracking.

4.4.1 Delivered Products

1. **Mineral aggregated spectral abundance,** provided as a 10 band global image in GeoTiff format, EPSG:4326 at 0.5 x 0.5 degree resolution. Each channel contains the Aggregated Spectral Abundance (see section 4.2) of each EMIT mineral.

2. **Mineral aggregated spectral abundance uncertainty,** provided as a 10 band global image in GeoTiff format, in EPSG:4326 at 0.5 x 0.5 degree resolution. Each channel contains the EMIT mineral aggregated spectral abundance measurement uncertainty as defined in section 5.

Note that on delivery, products are provided as a single NetCDF file, with a corresponding quicklook. Please see the L3 User Guide for more product details.

4.4.2 Auxiliary Products

1. **Fractional cover,** provided as an *n* x *c* x 3 BIL interleave data cube, with *c* columns and *n* lines. Each channel contains the fractional cover as calculated by Monte Carlo SMA (see section 4.2.1).
2. **Fractional cover uncertainty,** provided as an *n* x *c* x 3 BIL interleave data cube, with *c* columns and *n* lines. Each channel contains the estimated uncertainty of the fraction cover, as defined in section 5.

5. Calibration, uncertainty characterization and propagation, and validation

Uncertainty characterization of the aggregated L3 product comes through a combination of uncertainty estimates from the L2B outputs and Monte Carlo SMA products, and is ultimately provided as a spectral abundance uncertainty for each EMIT mineral. To estimate the uncertainty of the Monte Carlo SMA results, we run 50 Monte Carlo simulations. During each simulation, the endmember selection is seeded differently (representing model error) and the reflectance is perturbed by a (per-wavelength) random deviation proportionate to the channelized reflectance uncertainty provided by L2A. The standard deviation of the soil fractional cover from the different simulations (σ_s^j) is then used as the uncertainty. These results are used to estimate the standard deviation of f_s, or σ_s.

Neglecting the uncertainty of the binary masking, and treating $SA_{i,j}^c$ uncertainty as random and independent, we can reduce relative ASA uncertainty (Ψ_{ASA}^i) to:

$$\Psi_{ASA}^i = \sqrt{\left(\frac{ASA_i}{\sum_{j=1}^m (1-m_j)}\right)^2 \left\{\sum_{j=1}^N (1-m_j)\left(\left(\frac{\Psi_{SA_j}^i}{SA_{i,j}}\right)^2 + \left(\frac{\sigma_s^j}{f_s^j}\right)^2\right)\right\}} \quad (4)$$

where $\Psi_{SA_j}^i$ is the spectral abundance uncertainty for spatial index *j* and EMIT mineral *i*, as calculated in L2B. Notably, due to the random and independence assumptions, uncertainty decreases as a square root of the number of unmasked, observed pixels within the half degree grid cell. Following the 50% grid cell coverage requirement, this corresponds to a scaling factor of $1.5e^{-3}$ at the equator.

While the independence and randomness assumptions are reasonable for the origins of the propagated uncertainty values for ASA (which stem from L2A), there are several other potential sources of uncertainty that are not considered here. These include:

- **Misidentification inside of the L2B spectral library.** If the mineral identification process in L2B mistakes a surface property for another mineral, this error would not be captured in the L2B outputs, and consequently is unaccounted for in the L3 output. This type of error is likely to have some form of spatial component, given the general spatial autocorrelation of land features, and consequently would likely not diminish by the ~$1.5e^{-3}$ factor shown

above. However, there is no way of estimating this type of error without more complete surface knowledge, which is itself an objective of this mission.

- **Uncertainty from unmeasured areas.** Areas not observed by EMIT, or that were covered by cloud, shadow, or particularly high aerosol levels at the time of observation will not be included in the ASA calculations above. Consequently, up to 50% of the surface minerology could be unaccounted for. Due to the expected spatial autocorrelation of surface mineral composition, it is nevertheless likely that mapped areas within each half degree pixel are reasonable estimates of the ASA. This is particularly true at the global scale, where it is unlikely that unmeasured areas are systematically correlated with a specific mineral type.

6. Constraints and Limitations

No constraints or limitations are imposed on the L3 gridded data product. All delivered data will have undergone quality control and should be considered valid calibrations up to the reported uncertainties in input parameters. Unanticipated data corruption due to factors outside the modeling, if discovered, will be reported in peer reviewed literature and/or addenda to this ATBD.

References

Ardila, D. R., Dennison, P., Green, R. O., Renzullo, J., Roberts, D. A., Thompson, D. R. Routine Production of a Terrestrial Ecosystem Product for Green Vegetation, Non-Photosynthetic Vegetation, and Substrate Fractions for AVIRIS, JPL Internal Report available on request, 2017.

Asner, Gregory P., and David B. Lobell. "A biogeophysical approach for automated SWIR unmixing of soils and vegetation." *Remote sensing of environment* 74.1 (2000): 99-112.

Clark, R. N., and Roush, T. L., 1984, Reflectance spectroscopy: Quantitative analysis techniques for remote sensing applications: Journal of Geophysical Research, 89, p. 6329-6340.

Dennison, P. E., Halligan, K. Q., & Roberts, D. A. (2004). A comparison of error metrics and constraints for multiple endmember spectral mixture analysis and spectral angle mapper. *Remote Sensing of Environment*, *93*(3), 359-367.

Dennison, P. E., & Roberts, D. A. (2003). Endmember selection for multiple endmember spectral mixture analysis using endmember average RMSE. *Remote sensing of environment*, *87*(2-3), 123-135.

Dennison, P.E., Qi, Y., Meerdink, S.K., Kokaly, R.F., Thompson, D.R., Daughtry, C.S., Quemada, M., Roberts, D.A., Gader, P.D., Wetherley, E.B. and Numata, I., 2019. Comparison of Methods for Modeling Fractional Cover Using Simulated Satellite Hyperspectral Imager Spectra. *Remote Sensing*, *11*(18), p.2072.

Keshava and J. F. Mustard, "Spectral unmixing," *IEEE signal processing magazine*, vol. 19, no. 1, pp. 44–57, 2002.

Lawson, C. and Hanson, R. 1995, Solving Least Squares Problems, 1st edn. (Society for Industrial and Applied Mathematics).

Li, L., Mahowald, N., Balkanski, Y., Connelly, D., Ginoux, P., Ageitos, M. G., Hamilton, D., Kalashnikova, O., Klose, M., Miller, R. L., Obiso, V., Paynter, D. and Perez Garcia-Pando, C.: Large contribution of hematite and geothite to uncertainty in dust direct radiative forcing, Atmos. Chem. Phys., 2020.

Okin, G. S., Roberts, D. A., Murray, B., & Okin, W. J. (2001). Practical limits on hyperspectral vegetation discrimination in arid and semiarid environments. *Remote Sensing of Environment*, *77*(2), 212-225.

Okin, Gregory S., and Juan Gu. "The impact of atmospheric conditions and instrument noise on atmospheric correction and spectral mixture analysis of multispectral imagery." *Remote Sensing of Environment* 164 (2015): 130-141.

Roberts, D., M. Smith, and J. Adams. "Green vegetation, nonphotosynthetic vegetation, and soils in AVIRIS data." *Remote Sensing of Environment* 44.2-3 (1993): 255-269.

Roberts, D., Gardner, M., Church, R., Ustin, S., Scheer, G., & Green, R. 1998, Remote Sensing of Environment, 65, 267.

Roth, Keely L., Philip E. Dennison, and Dar A. Roberts. "Comparing endmember selection techniques for accurate mapping of plant species and land cover using imaging spectrometer data." *Remote Sensing of Environment* 127 (2012): 139-152.

Scanza, R. A., Mahowald, N., Ghan, S., Zender, C. S., Kok, J. F., Liu, X., et al. (2015). Modeling dust as component minerals in the Community Atmosphere Model: development of framework and impact on radiative forcing. *Atmos. Chem. Phys., 15*(1), 537-561. http://www.atmos-chem-phys.net/15/537/2015/

Schaaf, A. N., Dennison, P. E., Fryer, G. K., Roth, K. L., & Roberts, D. A. (2011). Mapping plant functional types at multiple spatial resolutions using imaging spectrometer data. *GIScience & Remote Sensing*, *48*(3), 324-344.

Zanaga, D., Van De Kerchove, R., De Keersmaecker, W., Souverijns, N., Brockmann, C., Quast, R., Wevers, J., Grosu, A., Paccini, A., Vergnaud, S., Cartus, O., Santoro, M., Fritz, S., Georgieva, I., Lesiv, M., Carter, S., Herold, M., Li, Linlin, Tsendbazar, N.E., Ramoino, F., Arino, O., (2021). ESA WorldCover 10 m 2020 v100. https://doi.org/10.5281/zenodo.5571936